

The Polydispersity of α B-Crystallin Is Rationalized by an Interconverting Polyhedral Architecture

Andrew J. Baldwin,^{1,2,3,6,*} Hadi Lioe,⁵ Gillian R. Hilton,⁵ Lindsay A. Baker,^{2,4,6} John L. Rubinstein,^{2,4,6} Lewis E. Kay,^{1,2,3,6} and Justin L.P. Benesch^{5,*}

¹Department of Molecular Genetics

²Department of Biochemistry

³Department of Chemistry

⁴Department of Medical Biophysics

University of Toronto, 1 Kings College Circle, Toronto, ON M5S 1A8, Canada

⁵Department of Chemistry, Physical and Theoretical Chemistry Laboratory, University of Oxford, South Parks Road, Oxford, Oxfordshire, OX1 3QZ, UK

⁶Molecular Structure and Function Program, The Hospital for Sick Children Research Institute, 555 University Avenue, Toronto, ON M5G 1X8, Canada

*Correspondence: ajb204@pound.med.utoronto.ca (A.J.B.), justin.benesch@chem.ox.ac.uk (J.L.P.B.)

DOI 10.1016/j.str.2011.09.015

SUMMARY

We report structural models for the most abundant oligomers populated by the polydisperse molecular chaperone α B-crystallin. Subunit connectivity is determined by using restraints obtained from nuclear magnetic resonance spectroscopy and mass spectrometry measurements, enabling the construction of various oligomeric models. These candidate structures are filtered according to their correspondence with ion-mobility spectrometry data and cross-validated by using electron microscopy. The ensuing best-fit structures reveal the polyhedral architecture of α B-crystallin oligomers, and provide a rationale for their polydispersity and facile interconversion.

INTRODUCTION

Traditional structural biology approaches typically involve measurements that average over all species in solution. Elucidating the properties of the individual states within heterogeneous and dynamic protein assemblies therefore represents a significant challenge (Russel et al., 2009). For this reason, structural studies of the molecular chaperone α B-crystallin, which populates an ensemble of interconverting oligomeric states (Figure 1A), have met with considerable difficulties (Horwitz, 2009). The emergence of “hybrid” methods, which combine information from multiple sources, has provided new impetus to elucidating the structure and dynamics of molecular systems resistant to characterization by any single technique (Cowieson et al., 2008; Robinson et al., 2007). Here we demonstrate a strategy based on a combination of mass spectrometry (MS), solution-state nuclear magnetic resonance spectroscopy (NMR), ion-mobility spectrometry (IM), and electron microscopy (EM), together with prior X-ray crystallography data, to determine

the architecture of the individual oligomeric states comprising the heterogeneous α B-crystallin ensemble.

α B-crystallin is a mammalian member of the small heat shock proteins (sHSPs), a family of molecular chaperones found in organisms spanning all biological kingdoms (Haslbeck et al., 2005; McHaourab et al., 2009; van Montfort et al., 2001a). sHSPs are an integral part of the cellular proteostasis network (Balch et al., 2008), binding unfolding proteins and preventing their accumulation into potentially pathogenic (Dobson, 2003) or thermodynamically stable (Baldwin et al., 2011c) aggregates. α B-crystallin performs its protective role throughout the body, and its malfunction is consequently associated with a range of protein deposition maladies from cataract to Alzheimer's disease (Arrigo et al., 2007; Ecroyd and Carver, 2009; Sun and MacRae, 2005). Crystallographic and NMR studies of truncated forms have revealed both α B-crystallin and the eye-lens-specific isoform α A to be composed of a dimeric β sheet domain (Bagn ris et al., 2009; Clark et al., 2011; Jehle et al., 2009; Laganowsky et al., 2010; Laganowsky and Eisenberg, 2010), an arrangement also found within the wild-type oligomers (Alexander et al., 2008; Jehle et al., 2010).

Although the structure of the dimers that serve as the building block of the polydisperse α B-crystallin ensemble has recently been elucidated, how they assemble into the various oligomers remains unclear. Here we combine and correlate information from NMR, MS, IM, and EM experiments to interrogate the oligomeric distribution populated by α B-crystallin. Specifically, the combination of MS and NMR experiments allows us to determine regions responsible for intersubunit connectivity, enabling the construction of oligomeric models. These candidate structures are assessed according to their correspondence with sizes of individual oligomers determined from IM-MS. The results are then cross-validated with EM data, and reveal that α B-crystallin exists not only in a range of stoichiometries but also a wide diversity of sizes. Moreover, by correspondence of our models with our IM-MS data, we isolate the likely architectures of highly populated oligomers of the protein. Notably, these structures provide an immediate rationale as to how this protein populates a polydisperse and interconverting ensemble of oligomers at equilibrium.

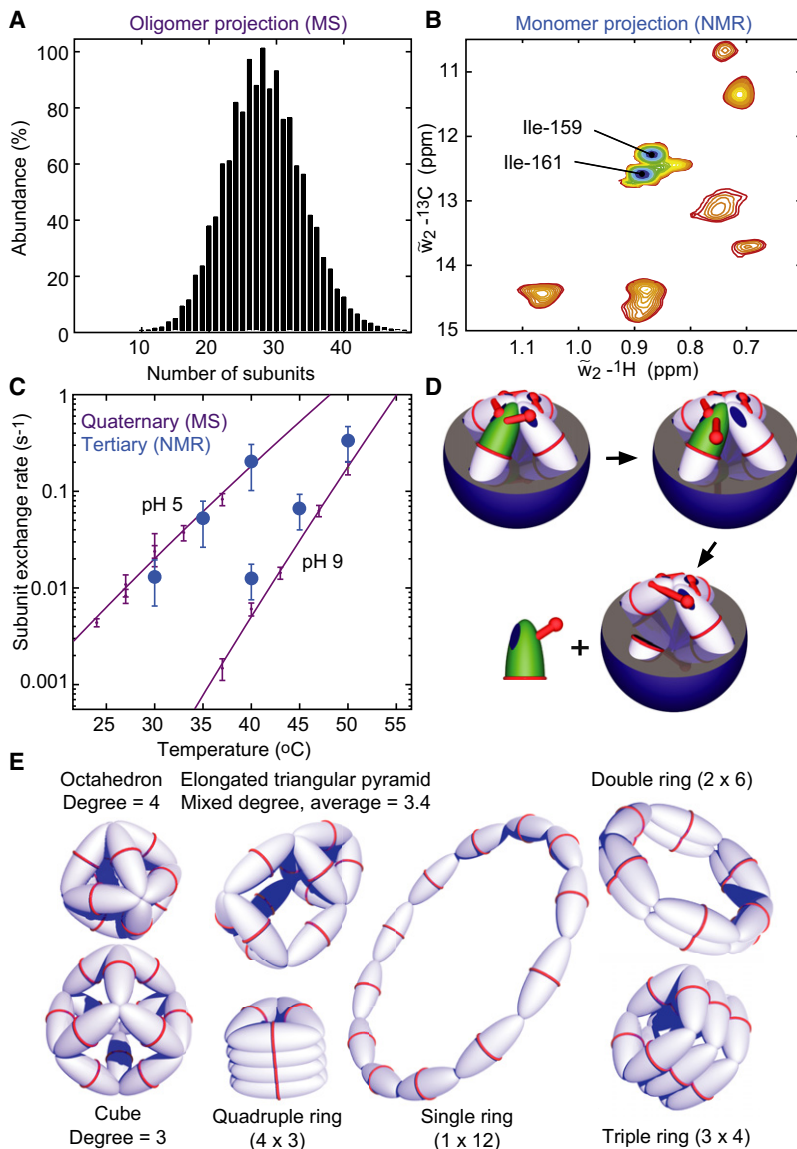


Figure 1. Polydispersity and Dynamics of α B-Crystallin as Probed by MS and NMR

MS can report on the oligomeric ensemble, whereas the NMR approach provides information about the tertiary structure of individual monomeric constituents. MS experiments show that this protein exists as a range of oligomeric forms containing between approximately 10 and 40 subunits (A) (Baldwin et al., 2011a). Methyl-TROSY NMR spectra show a single peak for each of the nine isoleucine residues, revealing that the monomers exist in a single conformation (B). The peaks corresponding to I159/161 in the C-terminal IXI motif undergo millisecond dynamics as measured by NMR relaxation dispersion experiments (Baldwin et al., 2011b). When the exchange rates are interpreted in terms of two coincident transitions that break intersubunit interactions involving C termini, the rates are in extremely good agreement with the global subunit exchange rate as measured by MS (C) (Baldwin et al., 2011b). Oligomers are assembled such that each monomer donates and receives a C terminus from neighboring monomers. The correlation shown in (C) demonstrates that the dissociation (green) of a monomer from any oligomer proceeds via an intermediate that has only one of the two C termini (red) firmly attached (D). A number of types of α B-crystallin oligomer models can be envisioned that meet these connectivity requirements. For a 24-mer, polyhedra of degree 3 (cube), 4 (octahedron), and mixed-degree (elongated triangular pyramid, degree 3.4) and single (1 ring of 12 dimers), double (2×6), triple (3×4), and quadruple (4×3) ring structures are illustrated (E). It should be noted that the double ring can be considered as a hexagonal prism, missing the edges connecting the two hexagonal faces together. See also Figure S1. Error bars in (C) were estimated by taking the standard error of the mean from repeated measurements and from the error in the fitting parameters from the appropriate χ^2 surfaces (Baldwin et al., 2011a, 2011b).

NMR experiments that show a single resonance for each probe in the protein core (Jehle et al., 2010) and Ile methyl-TROSY NMR experiments conducted in solution at physiological temperatures, where the number of cross-peaks

matches the number of Ile residues in the protein (Figure 1B) (Baldwin et al., 2011b).

Breaking of C-Terminal Interactions Is Rate Limiting in Subunit Exchange

Paramagnetic relaxation enhancement NMR experiments establish that the C terminus of each monomer makes interdimer contacts within the oligomer, and relaxation dispersion NMR measurements identify that the C terminus transitions between a pair of conformations on a millisecond timescale (Baldwin et al., 2011b).

The rate of subunit exchange, as determined with MS, and the rate of interconversion between C-terminal conformations, established by NMR, are in good agreement when the NMR data are interpreted in terms of a model in which the dissociation of a monomer from the oligomer occurs at the same rate as coincident transitions of two C termini (Figure 1C) (Baldwin et al.,

RESULTS AND DISCUSSION

Equivalent α B-Crystallin Monomers Establish a Dynamic Polydisperse Ensemble of Oligomers

MS is a well-established means for elucidating the stoichiometry of protein assemblies (Benesch et al., 2007; Heck, 2008; Sharon and Robinson, 2007), with the high resolution of separation allowing both the identification of individual components comprising a polydisperse ensemble and the quantification of their relative proportions (Benesch and Ruotolo, 2011). Our measurements of full-length α B-crystallin reveal a broad oligomeric distribution spanning 10- to 40-mers, in which monomers are free to “hop” between oligomers (Figure 1A). Monomers assemble into oligomers via both inter- and intradimer interactions, the energetics and kinetics of which have been shown to be independent of stoichiometry (Baldwin et al., 2011a). The equivalence of each monomer within the oligomers is further supported by solid-state

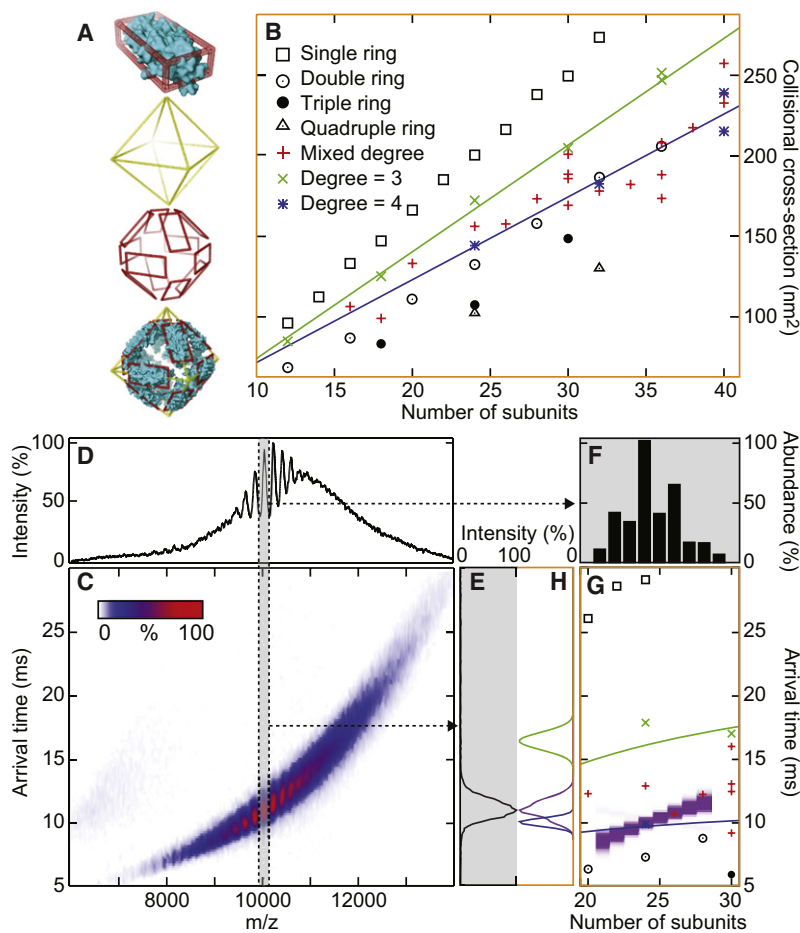


Figure 2. Combined Tandem-MS and IM-MS Approach to Interrogate the Polydisperse α B-Crystallin Ensemble

Candidate models are constructed by combining high-resolution structures of the dimeric building block with polyhedral scaffolds, shown here for an octahedron (A). This allows the construction of a database of putative structures of a given number of subunits and calculated CCS (B). To a good approximation, the CCS varies linearly with the number of monomers when degree is held constant. An IM-MS spectrum of α B-crystallin obtained at a traveling-wave height of 12.5 V (C), and the corresponding summed mass spectrum (D), is characteristic of a broad range of oligomeric masses and sizes. The ATD of the peak at 10,000 m/z can be extracted (E) and the identity and relative abundances of the underlying oligomers determined from tandem-MS (F). The arrival times for the individual oligomers within this range can be calculated (G) from the CCSs of the various models (B), and by combination with their relative abundances (F) converted into theoretical ATDs (H). Comparison between the experimental (E) and calculated data (H) allows the determination of the best fit of candidate structures to the IM-MS data. Clearly, the ATD calculated assuming oligomers based on rings (black symbols in G) or degree 3 polyhedra (green) fit poorly, whereas those based on degree 4 polyhedra (blue) provide a reasonable approximation. The best fit between calculated and experimental ATDs was obtained by assuming a linear relation between CCS and the number of monomers (H, purple). This comparison is shown here for 12.5 V, but is performed globally over nine different traveling-wave heights (Figure S2B). The best-fitting parameters and corresponding uncertainties were derived from a Bayesian probability surface (G, purple shading; further details are in Figure 3). Throughout the figure, black and orange borders denote experimental and theoretical data, respectively. See also Figure S2.

2011b). This correlation of quaternary and tertiary dynamics reveals that the rate-limiting step of monomer dissociation from a parent oligomer is the concurrent breaking of two interdimer C-terminal interactions (Figure 1D). It should be noted that our comparison is based purely on kinetics and does not rule out that other interactions, such as those arising from the N terminus (Jehle et al., 2011), contribute to the overall thermodynamic stability of the oligomers.

Candidate Oligomer Structures Can Be Constructed Using Restraints Derived from Correlated Protein Dynamics

The results of our NMR and MS measurements provide strong structural restraints on oligomeric connectivity, motivating the construction of candidate α B-crystallin oligomer structures. These are based on the high-resolution structures of the protomeric dimer (Bagn ris et al., 2009; Clark et al., 2011; Jehle et al., 2010; Laganowsky et al., 2010; Laganowsky and Eisenberg, 2010), and satisfy the following three criteria derived from our combined data set (Baldwin et al., 2011a, 2011b): (1) all monomers must be in essentially equivalent environments; (2) oligomers are built up from dimeric building blocks; and (3) each monomer is constrained by a pair of C-terminal “cross-linking” interactions. This picture is consistent with the mode of oligomerization seen for some sHSPs from other organisms

(Kim et al., 1998; van Montfort et al., 2001b) and with spectroscopic experiments on wild-type α B-crystallin showing interdimer C-terminal contacts (Jehle et al., 2010; Pasta et al., 2004).

Examination of the organization of other oligomeric sHSPs suggests they can be represented as regular convex polyhedra or rings, with dimers comprising the edges, N termini sequestered inside, and C termini binding to adjacent subunits at the vertices (see Figure S1 available online). Such forms therefore represent an attractive scaffold for modeling sHSP structures (Figure 1E), with each polyhedral arrangement associated with two parameters: the number of edges and the average number of edges that converge at each vertex (the “degree”). Similarly, ring-based structures are defined by the number of edges in each ring and the number of rings. By placing structures of the dimeric α B-crystallin core along the edges of these scaffolds, candidate structures were constructed (e.g., the 24-mer octahedron; Figure 2A). All such models are consistent with cryo-EM studies of the heterogeneous α B-crystallin ensemble, which loosely resembles a sphere with reduced central electron density (Haley et al., 1998, 1999). The sizes of our models were assessed in silico in terms of a rotationally averaged collisional cross-section (CCS), a property found to increase substantially and predictably with both the number of edges and decreasing degree (Figure 2B; Table S2).

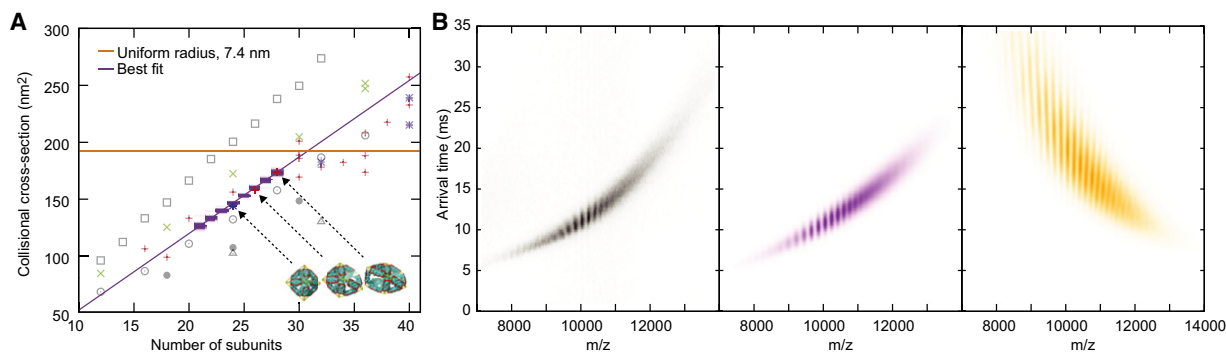


Figure 3. Size Distribution of α B-Crystallin Oligomers

A linear trend of CCS with oligomeric stoichiometry results in excellent agreement between experimental and calculated ATDs for the peak at 10,100 m/z (see Figure 2). The optimal gradient and intercept, and associated error surface, were determined from a global analysis (Figures S2B–S2E) and reveal a clear increase in CCS as a function of the number of subunits (A, purple shading). The CCS of each oligomeric state was determined to a precision of 3%. The structures that lie within these error bounds are indicated, and discussed in Figure 5. The linear trend observed was extrapolated across the entire range of oligomeric states observed in MS data, \sim 10–40 subunits (purple line), and an IM-MS spectrum based on this trend was calculated (B, purple). The agreement between this spectrum and the experimental data (B, black) was excellent, suggesting that α B-crystallin adopts a wide range of oligomeric sizes. Alternatively, assuming that α B-crystallin oligomers adopt structures of equal approximate radius, 7.4 nm (Jehle et al., 2011; Peschek et al., 2009) (A, orange line), results in a back-calculated IM-MS spectrum based in very poor agreement with our data (B, orange). It is apparent therefore that the oligomeric states populated by α B-crystallin at equilibrium adopt a diverse range of sizes.

Discriminating between Models by Combined Tandem-MS and IM-MS

In order to distinguish between the candidate models for each oligomeric state, we employed IM-MS. This technique separates oligomers in the gas phase according to not only mass-to-charge (m/z) ratio but also on their ability to traverse a cell of inert gas under the influence of a weak electric field (Ruotolo et al., 2008). The ensuing arrival-time distribution (ATD) is directly related to the CCS of the oligomers. An IM-MS spectrum of α B-crystallin reveals a band of signal spanning arrival times of 5 to 25 ms and 7,000–13,000 m/z (Figure 2C). The line projection of the m/z dimension does not display multiple distinct charge-state series but rather unresolved signal stemming from the broad distribution of oligomers comprising the α B-crystallin ensemble (Figure 2D) (Aquilina et al., 2003). As a result of these overlapping charge states, we cannot obtain CCSs for the individual oligomers directly from this spectrum.

To overcome the challenge posed by this heterogeneity, we developed a combined IM-MS and tandem-MS strategy. In our experiment, we obtain an ATD for the protein assemblies in an m/z range of interest, and in parallel identify the oligomers and their relative populations via tandem-MS. Specifically, we interrogated the peak centered at 10,100 m/z and 11.5 ms, which arises from a subset of oligomers, each carrying twice as many charges as subunits (Figure 2E). Tandem-MS of this peak, performed as described previously (Aquilina et al., 2003), reveals that the underlying subpopulation of oligomers consists largely of 24-mers, 26-mers, and 28-mers (Figure 2F).

In parallel to these experiments, we calculated the expected arrival times of our polyhedral models in silico based on their CCSs (Figure 2G). This allows a direct comparison of the experimental ATD of our selected subpopulation of α B-crystallin oligomers (Figure 2E) to ATDs calculated from specified CCS values, weighted according to the relative ratios of each oligomer within the selection (Figure 2H). The family of models based on degree 3 polyhedra (green) correspond very poorly to the experimental

data (black). By contrast, those based on degree 4 (blue) were found to be in reasonable agreement, suggesting that α B-crystallin has a tendency to adopt oligomeric architectures in which four dimers meet at each vertex. We have also calculated the best fit of the experimental ATD data to a model assuming a linear correlation of CCS with stoichiometry (Figure 2G, purple). This comparison is performed for the complete data set, obtained at nine different traveling-wave heights, and the data fitted globally (Figure S2B), and provides excellent agreement (Figure 2H).

From our fit of experimental and calculated ATDs, we obtain the optimal linear trend of CCS with the number of subunits (Figure 3A, purple band), with estimates of individual oligomer sizes extractable with uncertainties in CCSs of under 3% (Figures S2C–S2E). This relationship can be extrapolated across the entire range of oligomeric states observed in our MS data (Figure 1A), suggesting that oligomers range in CCSs between 50 and 250 nm² (Figure 3A, purple line). To validate our fit, we used this extrapolation, in combination with our knowledge of the oligomeric distribution (Figure 1A), to back-calculate an IM-MS spectrum for the entire range of oligomers (Figure 3B, purple). This matches the experimental spectrum (Figure 3B, black) very well. For comparison, we calculated an IM-MS spectrum if there were no trend in CCS with the number of subunits but rather all oligomers were of the same approximate size (Figure 3B, orange). In this case, the signal in the IM-MS spectrum is skewed such that oligomers at lower m/z have much longer arrival times than those at high m/z , and is a very poor reproduction of our data. Combined, our IM-MS results demonstrate that the oligomeric states α B-crystallin populates span a wide range of sizes at equilibrium.

Cross-Validation of the Oligomeric Size Distribution by Means of EM

Some previous studies have been interpreted in terms of a single stoichiometry or with a very narrow size distribution (Jehle et al., 2011; Peschek et al., 2009). In contrast, here we not only find

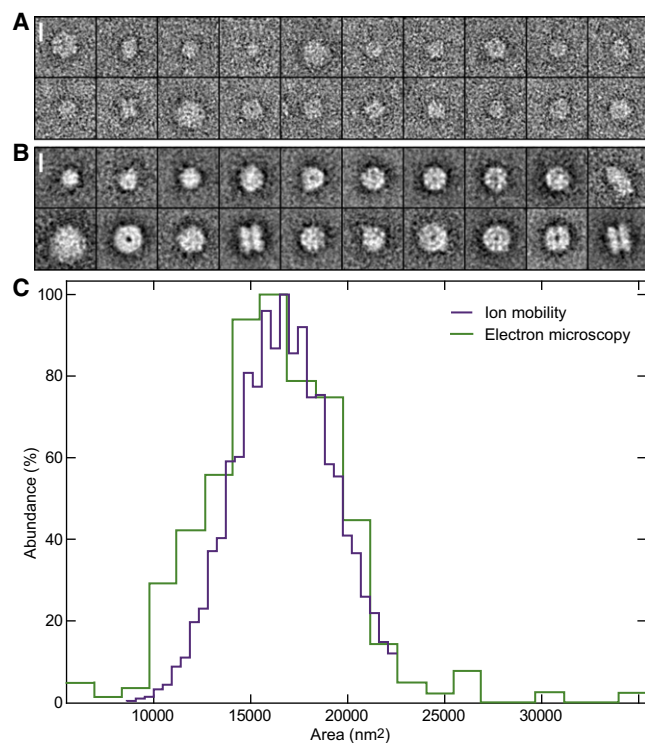


Figure 4. Correlating IM and EM Area Measurements

Negative-stain EM analysis was performed on α B-crystallin, with 20 particle images that represent the observed heterogeneity shown (A). Averages from classification into 200 classes reveal the diverse range of particle sizes, shapes, and symmetries present in the data (B, 20 classes shown, ordered by increasing area, clockwise from upper left). The scale bars represent 10 nm. A histogram of the EM class average areas was determined (C, green), and an equivalent histogram was calculated from the CCS values (C, purple), determined from the IM data (using best-fit values m and c ; see Figure 3A) and knowledge of the full oligomeric distribution (Figure 1A). These are in remarkably good agreement, demonstrating that the heterogeneity in size observed by IM is independently confirmed by the diversity in the sizes of particles observed by EM. See also Figure S3.

a range of oligomeric states but also a clear tendency for these to increase in size with the number of subunits, with the CCS of the 28-mer 20% larger than that of the 24-mer (Figure 3A). In order to cross-validate the findings from our gas-phase measurements to those obtained from more conventional means, we have compared our IM-derived size distribution with EM data (Figure 4). Over 3,000 negatively stained α B-crystallin particles were picked, and were found to display a range of apparent sizes (Figure 4A). Classification of these particles into 200 classes emphasizes the diversity of sizes and also reveals multiple symmetries (Figure 4B). To quantify the size of these particles, we determined the projected area of each class and compared the ensuing area distribution with that obtained by means of IM-MS (Figure 4C). This independently obtained distribution of particle size matches the overall CCS distribution very well, demonstrating that the gas-phase IM-MS measurements faithfully describe the solution-phase oligomers. Furthermore, the mean of our size distribution, which stems from a 28-mer under these conditions (Figure 1A), is in good agreement with

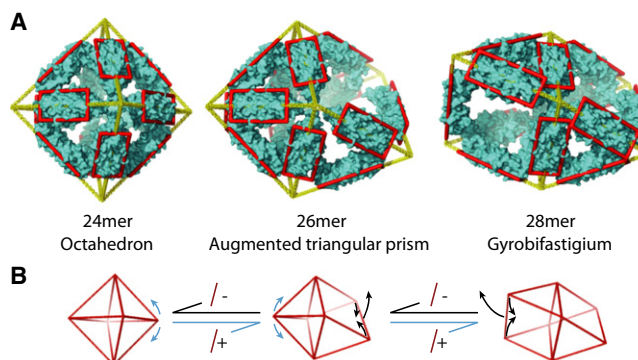


Figure 5. Oligomeric Structures of α B-Crystallin

The experimentally determined CCS measurements indicate unique structures for the 24-mer, 26-mer, and 28-mer (A). These structures are based on an octahedron, augmented triangular prism, and gyrobifastigium, respectively, which can interconvert simply by the insertion or removal of a single “dimeric” edge (B). The corresponding structures for the 23-mer, 25-mer, and 27-mer can be obtained by removing any one monomer. As the models were assembled from structures of a truncated α B-crystallin dimer, terminal regions are necessarily missing. As such, the central cavity is likely to be at least partly occupied, a consideration that does not substantially affect the CCS calculations from which the models are derived (Figure S1C).

that observed in other EM (Haley et al., 1998; Jehle et al., 2011; Peschek et al., 2009) and solution-phase scattering experiments (Jehle et al., 2010; Jehle et al., 2011; Peschek et al., 2009). Notably, classification of the α B-crystallin particles into fewer classes results in nearly identical copies of one “view” of the data in a much narrower size distribution, inconsistent with the diversity observed in the particles (Figure S3). In contrast to previous reports (Jehle et al., 2011; Peschek et al., 2009), these correlated IM and EM findings therefore demonstrate that the α B-crystallin oligomer ensemble is heterogeneous in terms of both mass and size.

Structural Basis of α B-Crystallin Heterogeneity and Quaternary Dynamics

Examination of the models whose CCSs best match our IM-MS data reveals likely architectures for the 24-mer, 26-mer, and 28-mer (Figure 3A). The best correspondence is obtained for the structures based on an octahedron, augmented triangular prism, and gyrobifastigium, respectively (Figure 5A). Examination of these polyhedral geometries provides a structural rationale for the facile interconversion of oligomers via the loss and addition of subunits. Opening one of the vertices of the octahedron and inserting an additional edge directly yields an augmented triangular prism (Figure 5B). Performing the same operation on the opposite vertex results in a gyrobifastigium. It is striking how the rearrangements required to achieve this are minimal, and that the environments of the subunits are very similar in all three structures. The only changes on the dimer level required to enable this are slight modifications in the angle made between the C terminus and the core domain, in a flexible region termed the “hinge loop” (Laganowsky et al., 2010). As such, these structures provide a clear means for understanding how α B-crystallin populates a range of oligomeric states at equilibrium.

Implications for the Structural Biology of Polydisperse Proteins

In conclusion, we have made use of a hybrid approach combining NMR and MS measurements to obtain a set of restraints that can be used to build models of α B-crystallin oligomers. IM data are used to derive the area distribution of oligomers, which is cross-validated by means of EM, and allow us to extract the sizes of the most populated stoichiometries. Comparison of the IM-MS data with our models of α B-crystallin reveals a set of candidate structures, which in themselves provide a rationale for how this important protein can interconvert between oligomeric states via only relatively minor structural rearrangements. Critical to the process is the very high two-dimensional separation, in terms of size and mass, afforded by combining tandem-MS with IM-MS. The methodology presented can readily be applied to the structure determination of other polydisperse proteins, which are among the most challenging targets for structural biology.

EXPERIMENTAL PROCEDURES

α B-crystallin was expressed in *Escherichia coli* and purified using standard methods (Meehan et al., 2007). Samples of the protein were analyzed using a combination of NMR (Sprangers et al., 2007), nano-electrospray MS (Hernández and Robinson, 2007), and IM-MS (Ruotolo et al., 2008) approaches developed to enable the study of large protein assemblies.

MS and NMR Correlation

To obtain the determinants of oligomeric assembly, we probed the quaternary and tertiary dynamics of α B-crystallin using a combination of MS and NMR. MS experiments were performed at a range of temperatures and pHs in 200 mM ammonium acetate and at a total monomer concentration of 50 μ M. Equilibrium oligomer distributions were obtained by means of a collision-induced dissociation MS (MS°) approach, performed and analyzed as described previously (Baldwin et al., 2011a) (Figure 1A). In order to determine the kinetics of subunit exchange, α B-crystallin was incubated with its isoform α A-crystallin, and the time dependence of the MS° spectra was monitored (Aquilina et al., 2005). These time courses were interpreted in terms of individual monomers mediating subunit exchange, allowing the extraction of the global subunit exchange rates (Baldwin et al., 2011a) (Figure 1C). NMR ^{13}C - 1H correlation spectra of Ile methyl-labeled ($^{13}CH_3$ - and otherwise $^{12}C/^2H$ -labeled) α B-crystallin were acquired as described previously (Baldwin et al., 2011c) (Figure 1B), with the intense correlations localized to the C-terminal IXI motif by mutagenesis. To probe and determine the rate constant for a transition between a ground and excited state, single-quantum carbon relaxation dispersion profiles were acquired (Lundström et al., 2007) and analyzed according to a two-state model as described previously (Baldwin et al., 2011c).

IM-MS Measurements

To interrogate the structure of α B-crystallin oligomers, we performed IM-MS measurements to obtain ATDs, and thereby CCSs, which can be used as restraints in topological modeling of protein assemblies (Politis et al., 2010; Pukala et al., 2009). IM-MS measurements were obtained at pH 7, 200 mM ammonium acetate, and a total monomer concentration of 50 μ M, using a Synapt G1 high-definition MS (HDMS) system (Waters UK) (Pringle et al., 2007), which effects IM separation with traveling direct current waves (Giles et al., 2004). The instrument parameters used were: nano-electrospray capillary 1.5 kV; sample cone 15 V; extractor cone 0.6 V; trap collision "energy" 15 V; source backing pressure 5.1 mbar; trap pressure 3.4×10^{-2} mbar (argon); time-of-flight (ToF) pressure 8.5×10^{-7} mbar; IM cell 0.43 mbar (nitrogen). Data were obtained at nine different wave heights from 10.5 to 14.5 V, with the wave velocity kept constant at 300 m/s.

CCS Calibration

To convert between the experimentally determined arrival time t_a and CCS for ions of charge Z in a traveling-wave instrument, the following relationship was used (Ruotolo et al., 2008):

$$CCS(t_d) = a + Zbt_d^c,$$

where t_d , the drift time, is given by $t_a - t_0$, t_a is the arrival time, and t_0 , the time spent between the IM cell and ToF analyzer, was $0.0008 \times \sqrt{(m/z)}$ for our experiments. The variables a , b , c were determined from measurements of calibrant protein complexes at each wave height (Table S1). Two monodisperse sHSPs, *Mj*HSP16.5 (Kim et al., 1998) and *Ta*HSP16.9 (van Montfort et al., 2001b), were chosen as reference proteins, as not only are they large protein assemblies of comparable mobility to α B-crystallin (Shvartsburg and Smith, 2008) but also, by having high sequence and structure homology to α B-crystallin, have similar propensity for any structural rearrangement upon gas-phase activation (Benesch, 2009; Benesch et al., 2006). Reference measurements for *Mj*HSP16.5 and *Ta*HSP16.9 were obtained on a separate Synapt G1 HDMS system equipped with a linear drift tube, which allows CCS determination without the need for calibration and has enabled the generation of a database for a range of protein assemblies (Bush et al., 2010).

Model Building

Our candidate models for even stoichiometries were constructed using home-built python code according to a set of four criteria based on our combined NMR and MS results (Baldwin et al., 2011a, 2011b) and the literature: (1) all monomers must be in essentially equivalent environments; (2) oligomers are built up from dimeric building blocks; (3) each monomer is held in place by a pair of C-terminal interactions; and (4) the oligomers have ring-like or polyhedral topology. As such, we have constructed a set of models based on combining the α B-crystallin dimer Protein Data Bank (PDB) ID code 2WJ7 (Bagnéris et al., 2009) with a database of different topological scaffolds (Table S2). The database of structural models comprised 64 regular polyhedra and rings ranging from 6 to 25 edges. Alternative dimer structures, or rotations thereof, make little difference to the CCS of the models (Table S3). Similarly, despite the models being constructed from dimers missing the terminal regions of sequence, this does not affect the CCS of the oligomers significantly (Figure S1C).

To construct the oligomer, initially a cuboidal box is generated with dimensions such that it encloses the α B-crystallin dimer. Equivalent boxes are placed on each edge of the candidate polyhedron, with the long edges of the box collinear to the edge of the polyhedron (Figure 2A). The resulting model is then adjusted such that the dimeric subunits in each box are within 2 Å of touching. Such an arrangement naturally allows the C-terminal interactions to form via association of adjacent monomers at the vertices of the polyhedron. The output that is generated is a PDB file whose CCS can be calculated in silico (see below) for comparison with experimental measurements. Structures of odd stoichiometries can be obtained by removing any monomer from the corresponding oligomer with one additional subunit.

CCS Calculation

CCS values from PDB files were calculated using CCSCalc (Williams et al., 2009) (Waters UK), which employs a projection approximation (PA) algorithm (Mack, 1925; von Helden et al., 1993). Although such CCS_{PA} values derived from crystal structures are known to slightly underestimate the measured CCS of protein assemblies (CCS_{Exp}) (Utrecht et al., 2010), they are very well correlated according to $CCS_{Exp} = (1.16 \pm 0.02) \times CCS_{PA}$ under the conditions employed here (Figure S3A). As such, through simple scaling, we can make direct comparisons between CCSs determined from our models and our measurements (Benesch and Ruotolo, 2011).

Arrival-Time Comparison

The shape of the drift time distribution for a single species is dictated by several factors that lead to an essentially Gaussian peak whose full width at half maximum (FWHM) height, Δt_d , scales linearly with drift time, t_d , for ions of similar mobility (Shvartsburg and Smith, 2008). This can be interpreted in terms of CCS using the calibration equation described above, and the quantity $CCS_0/\Delta CCS_{FWHM}$ therefore scales with charge, Z , and drift time according to

$$\frac{CCS_0}{\Delta CCS_{FWHM}} = \frac{\frac{a}{Zbt_d^c} + 1}{\left(1 + \frac{1}{2\kappa}\right)^c - \left(1 - \frac{1}{2\kappa}\right)^c} = \kappa_{CCS}(t_d),$$

where the resolving power $\kappa = t_d/\Delta t_d$. When a distribution of N types of ions of relative abundance A_i is studied, the distribution $D(t_d)$ of drift times is therefore given by

$$D(t_d) = \sum_{i=0}^N A_i \exp\left(-4 \ln(2)\kappa_{CCS}^2 \frac{(CCS(t_d) - CCS_i)^2}{CCS_i^2}\right),$$

where CCS_i is the CCS of species i . To a first approximation, we assume that the CCS varies linearly with oligomer size according to $CCS = mN + c$, where N is the number of monomers in an oligomer and m and c are free parameters. This is in part justified by the observation that linear relationships between CCS and the number of monomers arise when degree is held constant (Figure 2B), and allows ATDs to be calculated at a given wave height as a function of the three parameters m , c , and κ . By minimizing the least square residual between the experimental and calculated ATDs simultaneously at nine different wave heights, the best-fitting values of m , c , and κ were determined. In this way, individual oligomer CCS values could be derived, with their corresponding uncertainties (Figure 2G, purple; Figure S2). Home-written c++ code using a Levenberg-Marquardt algorithm was found to reliably perform this minimization, and is available on request. The experimentally measured CCS values were compared to those calculated from structural models (Figure 2G; Table S2) in order to determine which models best represent the structures of α B-crystallin oligomers (Figure 2I).

Calculation of IM-MS Spectra

Simulation of IM-MS spectra was based on an approach described previously (Sobott et al., 2002), as follows. Each oligomer was converted into a charge state series of Gaussian shape in charge space. Each such Gaussian was centered on an average charge state Z_{AV} given by $Z_{AV} = 0.0467M^{0.533}$, where M is the mass of the oligomer (Stengel et al., 2010), with the FWHM of each Gaussian given a value of 3.3 (Sobott et al., 2002) and a height proportional to its relative abundance in the distribution of oligomers (Figure 1A). This relation therefore provides a means to evaluate the relative contribution of each charge state to the final spectrum. Individual peaks were modeled as a two-dimensional Gaussian function, centered on M/Z_{AV} , and the arrival time given by the CCS (Figure S2F) converted into an arrival time as described above.

Negative-Stain Electron Microscopy

α B-crystallin at a concentration of 5 μ M (monomer) was stained with 2% uranyl acetate as described previously (Rubinstein and Walker, 2002), but without a second application of methylamine tungstate. Images were recorded using a Tecnai F20 microscope (FEI) equipped with a field emission gun and operated at 200 kV, 50,000 \times magnification, and nominal defoci between 0.3 and 1 μ m. SO-163 electron film (Kodak Canada) was used as the recording medium, and films were developed for 12 min in full-strength Kodak D19. Micrographs were digitized with an Intergraph PhotoScan densitometer using a 7 μ m step size. Images were averaged 2×2 to give a final pixel size of 2.8 \AA . Individual particles (3,422) were selected and windowed in 128×128 pixel boxes with MRC image analysis software (Crowther et al., 1996). Images were band-pass filtered between 700 and either 20 or 12 \AA , as described below, before alignment and classification with SPIDER (Frank et al., 1996).

Preliminary single-particle analysis using a small number of class averages (ca. 20–30) filtered to 12 \AA before alignment and classification (Jehle et al., 2011; Peschek et al., 2009) produced an apparently homogeneous data set (Figure S3), inconsistent with the heterogeneity observed in the particles. This behavior was reduced by separation of the data set into a larger number of classes, up to a limit of ~ 300 , whereupon the number of particle images constrained the improvement in signal-to-noise ratio obtained through averaging. As a result, 200 class averages were generated, as this number displayed the heterogeneity observed in the raw images and maintained sufficient signal-to-noise ratios for analysis. Alignment was found to be improved when images were band-pass filtered to 20 \AA . In these classes, a range of particle sizes, symmetries, and shapes were observed.

To quantify the heterogeneity in particle size observed in the data set, the area of each class average was estimated by counting the number of pixels above a threshold corresponding to 30% of the maximum image intensity, a value sufficient to reliably exclude background pixels. This method requires no assumptions about the shape, symmetry, or internal features of each class average. To scale this area to one that can be compared to other techniques, where internal features or different dimensions are less easily observed, the rotationally averaged radius of each class average was measured. The average radius was found to be 72 \AA (an estimate for the uncertainty on each radius measurement was ± 4 \AA), a value in excellent agreement with previous EM studies (Haley et al., 1998; Jehle et al., 2011; Peschek et al., 2009) as well as solution-phase scattering measurements (Jehle et al., 2010, 2011; Peschek et al., 2009).

SUPPLEMENTAL INFORMATION

Supplemental Information includes three figures and three tables and can be found with this article online at doi:10.1016/j.str.2011.09.015.

ACKNOWLEDGMENTS

We thank Carol Robinson, Antoni Borysik, and Art Laganowsky (University of Oxford); Christine Slingsby (Birkbeck College); and Flemming Hansen, Julie Forman-Kay, and Hong Lin (University of Toronto) for stimulating discussions. This work was supported by grants from the CIHR and NSERC (L.E.K.) and Royal Society (J.L.P.B.). A.J.B. is a CIHR postdoctoral fellow, H.L. was an EMBO fellow, L.E.K. holds a Canadian Research Chair in Biochemistry, and J.L.P.B. is a Royal Society University Research Fellow.

Received: August 3, 2011

Revised: September 15, 2011

Accepted: September 17, 2011

Published: December 6, 2011

REFERENCES

- Alexander, N., Bortolus, M., Al-Mestarihi, A., Mchaourab, H., and Meiler, J. (2008). De novo high-resolution protein structure determination from sparse spin-labeling EPR data. *Structure* 16, 181–195.
- Aquilina, J.A., Benesch, J.L., Bateman, O.A., Slingsby, C., and Robinson, C.V. (2003). Polydispersity of a mammalian chaperone: mass spectrometry reveals the population of oligomers in α B-crystallin. *Proc. Natl. Acad. Sci. USA* 100, 10611–10616.
- Aquilina, J.A., Benesch, J.L.P., Ding, L.L., Yaron, O., Horwitz, J., and Robinson, C.V. (2005). Subunit exchange of polydisperse proteins: mass spectrometry reveals consequences of α A-crystallin truncation. *J. Biol. Chem.* 280, 14485–14491.
- Arrigo, A.P., Simon, S., Gibert, B., Kretz-Remy, C., Nivon, M., Czekalla, A., Guillet, D., Moulin, M., Diaz-Latoud, C., and Vicart, P. (2007). Hsp27 (HspB1) and α B-crystallin (HspB5) as therapeutic targets. *FEBS Lett.* 581, 3665–3674.
- Bagn ris, C., Bateman, O.A., Naylor, C.E., Cronin, N., Boelens, W.C., Keep, N.H., and Slingsby, C. (2009). Crystal structures of α -crystallin domain dimers of α B-crystallin and Hsp20. *J. Mol. Biol.* 392, 1242–1252.
- Baich, W.E., Morimoto, R.I., Dillin, A., and Kelly, J.W. (2008). Adapting proteostasis for disease intervention. *Science* 319, 916–919.
- Baldwin, A.J., Lioe, H., Robinson, C.V., Kay, L.E., and Benesch, J.L.P. (2011a). α B-crystallin polydispersity is a consequence of unbiased quaternary dynamics. *J. Mol. Biol.* 413, 297–309.
- Baldwin, A.J., Hilton, G.R., Lioe, H., Bagn ris, C., Benesch, J.L.P., and Kay, L.E. (2011b). Quaternary dynamics of α B-crystallin as a direct consequence of localised tertiary fluctuations in the C-terminus. *J. Mol. Biol.* 413, 310–320.
- Baldwin, A.J., Knowles, T.P., Tartaglia, G.G., Fitzpatrick, A.W., Devlin, G.L., Shammis, S.L., Waudby, C.A., Mossuto, M.F., Meehan, S., Gras, S.L., et al. (2011c). Metastability of native proteins and the phenomenon of amyloid formation. *J. Am. Chem. Soc.* 133, 14160–14163.

- Benesch, J.L.P. (2009). Collisional activation of protein complexes: picking up the pieces. *J. Am. Soc. Mass Spectrom.* *20*, 341–348.
- Benesch, J.L.P., and Ruotolo, B.T. (2011). Mass spectrometry: come of age for structural and dynamical biology. *Curr. Opin. Struct. Biol.* *21*, 641–649.
- Benesch, J.L.P., Ruotolo, B.T., Simmons, D.A., and Robinson, C.V. (2007). Protein complexes in the gas phase: technology for structural genomics and proteomics. *Chem. Rev.* *107*, 3544–3567.
- Benesch, J.L.P., Aquilina, J.A., Ruotolo, B.T., Sobott, F., and Robinson, C.V. (2006). Tandem mass spectrometry reveals the quaternary organization of macromolecular assemblies. *Chem. Biol.* *13*, 597–605.
- Bush, M.F., Hall, Z., Giles, K., Hoyes, J., Robinson, C.V., and Ruotolo, B.T. (2010). Collision cross sections of proteins and their complexes: a calibration framework and database for gas-phase structural biology. *Anal. Chem.* *82*, 9557–9565.
- Clark, A.R., Naylor, C.E., Bagn ris, C., Keep, N.H., and Slingsby, C. (2011). Crystal structure of R120G disease mutant of human α B-crystallin domain dimer shows closure of a groove. *J. Mol. Biol.* *408*, 118–134.
- Cowieson, N.P., Kobe, B., and Martin, J.L. (2008). United we stand: combining structural methods. *Curr. Opin. Struct. Biol.* *18*, 617–622.
- Crowther, R.A., Henderson, R., and Smith, J.M. (1996). MRC image processing programs. *J. Struct. Biol.* *116*, 9–16.
- Dobson, C.M. (2003). Protein folding and misfolding. *Nature* *426*, 884–890.
- Ecroyd, H., and Carver, J.A. (2009). Crystallin proteins and amyloid fibrils. *Cell. Mol. Life Sci.* *66*, 62–81.
- Frank, J., Radermacher, M., Penczek, P., Zhu, J., Li, Y., Ladjadj, M., and Leith, A. (1996). SPIDER and WEB: processing and visualization of images in 3D electron microscopy and related fields. *J. Struct. Biol.* *116*, 190–199.
- Giles, K., Pringle, S.D., Worthington, K.R., Little, D., Wildgoose, J.L., and Bateman, R.H. (2004). Applications of a travelling wave-based radio-frequency-only stacked ring ion guide. *Rapid Commun. Mass Spectrom.* *18*, 2401–2414.
- Haley, D.A., Horwitz, J., and Stewart, P.L. (1998). The small heat-shock protein, α B-crystallin, has a variable quaternary structure. *J. Mol. Biol.* *277*, 27–35.
- Haley, D.A., Horwitz, J., and Stewart, P.L. (1999). Image restrained modeling of α B-crystallin. *Exp. Eye Res.* *68*, 133–136.
- Haslbeck, M., Franzmann, T., Weinfurter, D., and Buchner, J. (2005). Some like it hot: the structure and function of small heat-shock proteins. *Nat. Struct. Mol. Biol.* *12*, 842–846.
- Heck, A.J. (2008). Native mass spectrometry: a bridge between interactomics and structural biology. *Nat. Methods* *5*, 927–933.
- Hern andez, H., and Robinson, C.V. (2007). Determining the stoichiometry and interactions of macromolecular assemblies from mass spectrometry. *Nat. Protoc.* *2*, 715–726.
- Horwitz, J. (2009). α crystallin: the quest for a homogeneous quaternary structure. *Exp. Eye Res.* *88*, 190–194.
- Jehle, S., van Rossum, B., Stout, J.R., Noguchi, S.M., Falber, K., Rehbein, K., Oschkinat, H., Klevit, R.E., and Rajagopal, P. (2009). α B-crystallin: a hybrid solid-state/solution-state NMR investigation reveals structural aspects of the heterogeneous oligomer. *J. Mol. Biol.* *385*, 1481–1497.
- Jehle, S., Vollmar, B.S., Bardiaux, B., Dove, K.K., Rajagopal, P., Gonen, T., Oschkinat, H., and Klevit, R.E. (2011). N-terminal domain of α B-crystallin provides a conformational switch for multimerization and structural heterogeneity. *Proc. Natl. Acad. Sci. USA* *108*, 6409–6414.
- Jehle, S., Rajagopal, P., Bardiaux, B., Markovic, S., K hne, R., Stout, J.R., Higman, V.A., Klevit, R.E., van Rossum, B.J., and Oschkinat, H. (2010). Solid-state NMR and SAXS studies provide a structural basis for the activation of α B-crystallin oligomers. *Nat. Struct. Mol. Biol.* *17*, 1037–1042.
- Kim, K.K., Kim, R., and Kim, S.H. (1998). Crystal structure of a small heat-shock protein. *Nature* *394*, 595–599.
- Laganowsky, A., and Eisenberg, D. (2010). Non-3D domain swapped crystal structure of truncated zebrafish α A crystallin. *Protein Sci.* *19*, 1978–1984.
- Laganowsky, A., Benesch, J.L.P., Landau, M., Ding, L., Sawaya, M.R., Cascio, D., Huang, Q., Robinson, C.V., Horwitz, J., and Eisenberg, D. (2010). Crystal structures of truncated α A and α B crystallins reveal structural mechanisms of polydispersity important for eye lens function. *Protein Sci.* *19*, 1031–1043.
- Lundstr m, P., Vallurupalli, P., Religa, T.L., Dahlquist, F.W., and Kay, L.E. (2007). A single-quantum methyl 13 C-relaxation dispersion experiment with improved sensitivity. *J. Biomol. NMR* *38*, 79–88.
- Mack, E., Jr. (1925). Average cross-sectional areas of molecules by gaseous diffusion methods. *J. Am. Chem. Soc.* *47*, 2468–2482.
- McHaourab, H.S., Godar, J.A., and Stewart, P.L. (2009). Structure and mechanism of protein stability sensors: chaperone activity of small heat shock proteins. *Biochemistry* *48*, 3828–3837.
- Meehan, S., Knowles, T.P., Baldwin, A.J., Smith, J.F., Squires, A.M., Clements, P., Treweek, T.M., Ecroyd, H., Tartaglia, G.G., Vendruscolo, M., et al. (2007). Characterisation of amyloid fibril formation by small heat-shock chaperone proteins human α A-, α B- and R120G α B-crystallins. *J. Mol. Biol.* *372*, 470–484.
- Pasta, S.Y., Raman, B., Ramakrishna, T., and Rao, ChM. (2004). The IXI/V motif in the C-terminal extension of α -crystallins: alternative interactions and oligomeric assemblies. *Mol. Vis.* *10*, 655–662.
- Peschek, J., Braun, N., Franzmann, T.M., Georgalis, Y., Haslbeck, M., Weinkauff, S., and Buchner, J. (2009). The eye lens chaperone α -crystallin forms defined globular assemblies. *Proc. Natl. Acad. Sci. USA* *106*, 13272–13277.
- Politis, A., Park, A.Y., Hyung, S.J., Barsky, D., Ruotolo, B.T., and Robinson, C.V. (2010). Integrating ion mobility mass spectrometry with molecular modelling to determine the architecture of multiprotein complexes. *PLoS One* *5*, e12080.
- Pringle, S.D., Giles, K., Wildgoose, J.L., Williams, J.P., Slade, S.E., Thalassinou, K., Bateman, R.H., Bowers, M.T., and Scrivens, J.H. (2007). An investigation of the mobility separation of some peptide and protein ions using a new hybrid quadrupole/travelling wave IMS/oa-ToF instrument. *Int. J. Mass Spectrom.* *261*, 1–12.
- Pukala, T.L., Ruotolo, B.T., Zhou, M., Politis, A., Stefanescu, R., Leary, J.A., and Robinson, C.V. (2009). Subunit architecture of multiprotein assemblies determined using restraints from gas-phase measurements. *Structure* *17*, 1235–1243.
- Robinson, C.V., Sali, A., and Baumeister, W. (2007). The molecular sociology of the cell. *Nature* *450*, 973–982.
- Rubinstein, J., and Walker, J. (2002). ATP synthase from *Saccharomyces cerevisiae*: location of the OSCP subunit in the peripheral stalk region. *J. Mol. Biol.* *321*, 613–619.
- Ruotolo, B.T., Benesch, J.L.P., Sandercock, A.M., Hyung, S.J., and Robinson, C.V. (2008). Ion mobility-mass spectrometry analysis of large protein complexes. *Nat. Protoc.* *3*, 1139–1152.
- Russel, D., Lasker, K., Phillips, J., Schneidman-Duhovny, D., Vel zquez-Muriel, J.A., and Sali, A. (2009). The structural dynamics of macromolecular processes. *Curr. Opin. Cell Biol.* *21*, 97–108.
- Sharon, M., and Robinson, C.V. (2007). The role of mass spectrometry in structure elucidation of dynamic protein complexes. *Annu. Rev. Biochem.* *76*, 167–193.
- Shvartsburg, A.A., and Smith, R.D. (2008). Fundamentals of traveling wave ion mobility spectrometry. *Anal. Chem.* *80*, 9689–9699.
- Sobott, F., Benesch, J.L.P., Vierling, E., and Robinson, C.V. (2002). Subunit exchange of multimeric protein complexes. Real-time monitoring of subunit exchange between small heat shock proteins by using electrospray mass spectrometry. *J. Biol. Chem.* *277*, 38921–38929.
- Sprangers, R., Velyvis, A., and Kay, L.E. (2007). Solution NMR of supramolecular complexes: providing new insights into function. *Nat. Methods* *4*, 697–703.
- Stengel, F., Baldwin, A.J., Painter, A.J., Jaya, N., Basha, E., Kay, L.E., Vierling, E., Robinson, C.V., and Benesch, J.L. (2010). Quaternary dynamics and plasticity underlie small heat shock protein chaperone function. *Proc. Natl. Acad. Sci. USA* *107*, 2007–2012.
- Sun, Y., and MacRae, T.H. (2005). The small heat shock proteins and their role in human disease. *FEBS J.* *272*, 2613–2627.

Utrecht, C., Rose, R.J., van Duijn, E., Lorenzen, K., and Heck, A.J. (2010). Ion mobility mass spectrometry of proteins and protein assemblies. *Chem. Soc. Rev.* 39, 1633–1655.

van Montfort, R., Slingsby, C., and Vierling, E. (2001a). Structure and function of the small heat shock protein/ α -crystallin family of molecular chaperones. *Adv. Protein Chem.* 59, 105–156.

van Montfort, R.L., Basha, E., Friedrich, K.L., Slingsby, C., and Vierling, E. (2001b). Crystal structure and assembly of a eukaryotic small heat shock protein. *Nat. Struct. Biol.* 8, 1025–1030.

von Helden, G., Hsu, M.T., Gotts, N., and Bowers, M.T. (1993). Carbon cluster cations with up to 84 atoms: structures, formation mechanism, and reactivity. *J. Phys. Chem.* 97, 8182–8192.

Williams, J.P., Lough, J.A., Campuzano, I., Richardson, K., and Sadler, P.J. (2009). Use of ion mobility mass spectrometry and a collision cross-section algorithm to study an organometallic ruthenium anticancer complex and its adducts with a DNA oligonucleotide. *Rapid Commun. Mass Spectrom.* 23, 3563–3569.